Article

Properties of Antiferroelectric Mixtures Differing in the Amount of Added Racemate

Magdalena Urbańska [1,*] and Dorota Dardas [2]

1   Institute of Chemistry, Military University of Technology, ul. Sylwestra Kaliskiego 2, 00-908 Warsaw, Poland
2   Institute of Molecular Physics, Polish Academy of Sciences, ul. Mariana Smoluchowskiego 17, 60-179 Poznań, Poland; dardas@ifmpan.poznan.pl
*   Correspondence: magdalena.urbanska@wat.edu.pl

Abstract: Novel three-component liquid crystalline mixtures composed of chiral and achiral (racemic) liquid crystalline materials were designed and studied by polarizing optical microscopy, differential scanning calorimetry, and UV–VIS spectroscopy. The compositions of liquid crystalline mixtures were developed based on the composition of a two-component (binary) mixture marked as W-1000 with the following phase sequence: $Cr \leftrightarrow SmC_A^* \leftrightarrow SmC^* \leftrightarrow SmA^* \leftrightarrow Iso$. This mixture has an antiferroelectric (SmC_A^*) phase over a wide temperature range and exhibits a helical pitch inversion in this phase. All newly obtained mixtures occur in a wide temperature range of the SmC_A^* phase, while the ferroelectric (SmC^*) phase and the orthogonal (SmA^*) phase occur in a narrow temperature range. The new mixtures also have a very long helical pitch in the antiferroelectric phase and a short helical pitch in the ferroelectric phase.

Keywords: (S) enantiomers; racemate; mixtures; antiferroelectric phase; helical pitch

1. Introduction

Liquid crystal technology has significantly impacted many fields of science, engineering, and device technology. Applications for this unique type of material are continually being developed, and they continue to offer efficient answers to a wide range of issues. The liquid crystalline phases can be observed in organic compounds characterized by specific chemical structures. Liquid crystals can be divided into different categories. An essential division concerns how they are created. Thermotropic liquid crystals (TLC) are formed when solid crystals are heated; they can occur as enantiotropic or monotropic, depending on whether they pass through different mesophases as the temperature increases. Lyotropic liquid crystals (LLC) are created by being dissolved in an appropriate isotropic solvent that participates in the construction of this phase. Thermotropic liquid crystals are very often single compounds or mixtures thereof. However, lyotropic compounds are always solutions or systems of at least two compounds. An exciting example of the lyotropic liquid crystal is the amphiphilic crystal, created by molecules consisting of two parts with opposite properties—hydrophobic and hydrophilic [1]. Some mesogens, which are called amphotropics, may exhibit the properties of both phases. Due to the shape of the molecules, we can distinguish liquid crystals as calamitic (rod-like), discotic (disc-like), flat (board-like), pyramidal, circular, polychain, or dovetail. The thermotropic liquid crystals of elongated molecules are mainly subdivided into nematic and smectic mesophases. Nematic liquid crystals, marked with the symbol N, have the least ordered structure, and only have orientational order along the longitudinal axis of the molecules. This axis has a precisely defined direction, which we call the director, *n*. The molecules' average direction determines the system's optical axis. The molecules are parallel to some extent and can move in three directions but cannot rotate around the short axis. The center of gravity is isotropically distributed in all directions, as shown in Figure 1. Among the nematic phases, we can also distinguish chiral nematic phases, which are marked with the symbol N* and

are called cholesteric liquid crystals (ChLC). Unlike nematic achiral phases, they have a layered structure. A characteristic feature of cholesterics is that the center of gravity of the molecules in the layer is randomly located, and the layers are twisted towards each other by a certain small angle. As a result of the twisting of the layers, a helix is formed [1].
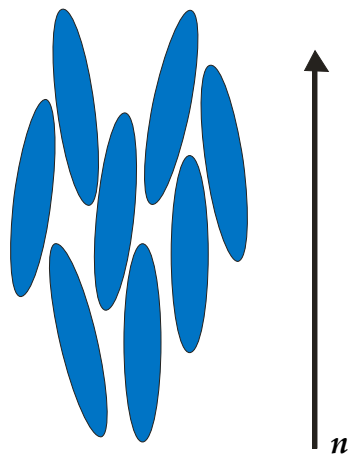

Figure 1. The arrangement of molecules in the nematic phase.

Liquid crystals belonging to smetics have a more ordered structure than nematics. In addition to orientational order, they also show positional order, which results in the formation of layers of molecules. Smectic liquid crystals include compounds with only a smectic phase or those that form a smectic phase at lower temperatures and a nematic phase at higher temperatures. The common feature of all classes is the layered structure. Still, they differ in the arrangement of molecules in the layer, the range and type of intermolecular interactions, and the range of positional and orientational ordering. Smectic phases are divided into orthogonal and oblique phases. There are many types of smectic phases, and most of the compounds synthesized by our research group (at the Military University of Technology) have A, C, and C_A phases. In the smectic A phase (SmA), the director and the optical axis are perpendicular to the layer surface but simultaneously parallel to the normal to layer, k, as shown in Figure 2.

Important applications have chiral smectic liquid crystals with ferroelectric and antiferroelectric phases [1–8]. When molecules are chiral, a macroscopic helical structure is created, characterized by the helical pitch, p. The phase that exhibits the ferroelectric properties is the chiral synclinic (SmC*) phase [9]. The molecules of this phase form a layered structure, the centers of gravity of the molecules are randomly distributed, and the molecules themselves are tilted by an angle of 13–45°. The subsequent layers are twisted. The structure of the SmC* phase allows for spontaneous polarization to occur. This phenomenon can be explained as follows: spontaneous polarization, P_s, is a vector representing symmetry breaking. If the properties of the liquid crystal are independent of the direction of the director, P_s, if present, must be locally perpendicular to *n*. In the case of the SmA phase, which has rotational symmetry, spontaneous polarization disappears, similar to the SmC phase, which has mirror symmetry. This symmetry is broken thanks to the chiral center present in the SmC* phase.

Chiral smectic phases with antiferroelectric properties were discovered in 1989 [10,11]. This phase differs from the ferroelectric phase in that two adjacent layers are opposed in the chiral anticlinic phase (SmC$_A$*).
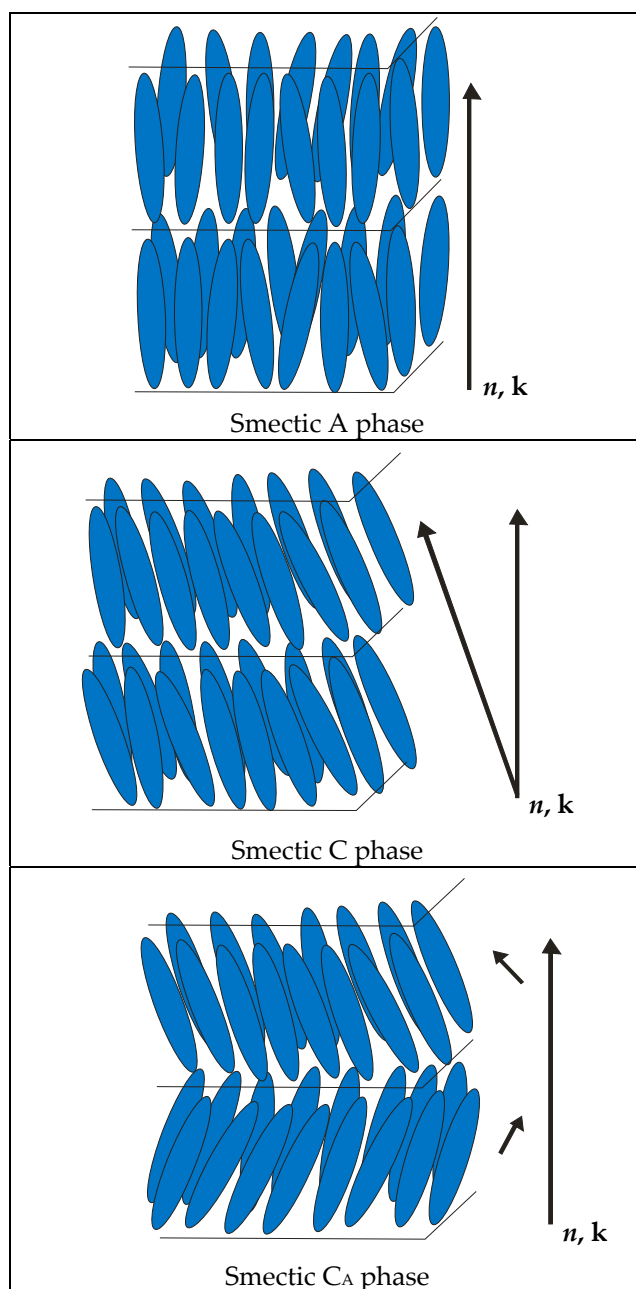
Figure 2. The arrangement of molecules in three smectic phases.

In many applications, liquid crystalline mixtures are used because single compounds are insufficient to obtain the desired properties [12–26]. It has been shown that the properties of their binary mixtures can be predicted by using mixtures of two liquid crystalline materials with the ferroelectric phase with previously known properties, such as viscoelastic properties [27,28]. Several dozen mixtures with excellent physicochemical and electro-optical properties have been prepared at the Military University of Technology Institute of Chemistry. One well-studied mixture, which shows a very wide orthoconic antiferroelectric phase and a very long helical pitch, is the binary mixture W-1000 [29–31] and its modifications [32–35]. Orthoconic antiferroelectric liquid crystals (OAFLCs) are compounds in which molecules are tilted in layers by 45°. In this case, the optical properties of the orthoconic antiferroelectrics change significantly [7,18,26,29,31–36]. The first publications on high-tilted compounds with the antiferroelectric phase appeared in the 1990s; a tilt angle of $\Theta \approx 40°$ was detected in siloxane liquid crystalline compounds. The
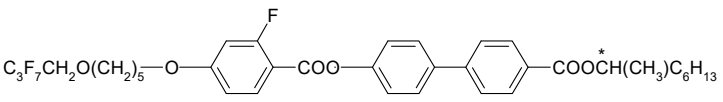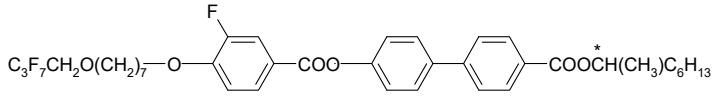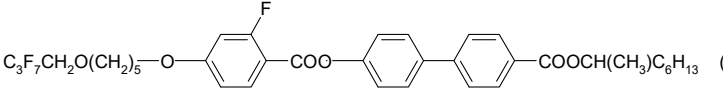
first orthoconics with antiferroelectric properties that were not dimers of two compounds were obtained at the Military University of Technology in the research group of Prof. R. Dąbrowski [2,3,7]. Compared to conventional antiferroelectric liquid crystalline materials, they have fewer structural defects in liquid crystalline cells. Studies have demonstrated excellent electro-optical properties of the mixture W-1000, including extraordinary optical contrast and optical switching without light leakage. All articles about this mixture either describe its properties or the properties after doping this mixture with some chiral compound(s) or racemate(s) (racemic equivalents of the components of this mixture have never been used as dopants). Usually, better properties have been observed after doping, and we used a completely different approach. Since the mixture has excellent properties, what will happen if it is partially racemized? We decided to replace one of the chiral components (dominant) in 50%, 25%, and 10% with the racemate, while the other chiral compound remained unchanged. We did not decide to replace one of the components at 100% with the racemate because then only one of the mixture's components would be in a chiral form.

In this work, we investigated how the amount of the added racemate affected the mixtures' mesomorphic and thermodynamic properties and helical pitch, and compared them with the base mixture.

2. Compositions of Mixtures

The basis for the preparation of the new mixtures with the acronyms W-462, W-463, and W-464 was the mixture W-1000. The formulas of all mesogens used to prepare the mixtures are presented in Table 1. A total of 100 mg of each new liquid crystalline mixture was prepared by weighing the appropriate amount of each component, heating them to the isotropic phase, and mixing them several times.

Table 1. All mixture components and phase transition temperatures (from DSC measurements) [36].

Acronyms	Structure of Enantiomers/Racemate
1.(S)	$C_3F_7CH_2O(CH_2)_5$—O—⟨F⟩—COO—⟨⟩—⟨⟩—COOCH*(CH_3)C_6H_{13}$ (S)
	Cr 28.1 SmC$_A$* (97.0) [&] SmA* 99.0 Iso
2.(S)	$C_3F_7CH_2O(CH_2)_7$—O—⟨F⟩—COO—⟨⟩—⟨⟩—COOCH*(CH_3)C_6H_{13}$ (S)
	Cr 37.4 SmC$_A$* 103.1 SmC* 104.3 SmA* 109.1 Iso
3.(R,S)	$C_3F_7CH_2O(CH_2)_5$—O—⟨F⟩—COO—⟨⟩—⟨⟩—COOCH(CH_3)C_6H_{13}$ (R,S)
	Cr 39.1 SmC$_A$ 84.1 SmC 95.1 Iso

[&] (monotropic transition).

Tables 2 and 3 show the compositions and percentages of the components of all mixtures. The synthesis of the components used to prepare all mixtures is described in [36,37]. All mesogens were synthesized using the same classical pathway by treating the chiral or achiral phenol with benzoic acid chloride in the presence of pyridine. The mesogens were purified using a combination of column chromatography and recrystallization. The purity was checked using a Shimadzu prominence chromatograph with an SPD-M20A diode array detector. All mesogens have a purity higher than 99%. MS data for the mesogens are provided in the Supplementary Materials, see Figures S1–S3. The purity of the mesogens was also checked using thin-layer chromatography (TLC).

Table 2. Weight composition of the base mixture W-1000.

Acronyms of Enantiomers	Weight Ratio [%]
1.(S)	52.52
2.(S)	47.48

Table 3. Weight compositions of the mixtures W-462, W-463, and W-464.

Mixtures	Acronyms of Enantiomers/Racemate	Weight Ratio [%]
W-462	1.(S)	26.26
	3.(R,S)	26.26
	2.(S)	47.48
W-463	1.(S)	39.39
	3.(R,S)	13.13
	2.(S)	47.48
W-464	1.(S)	47.27
	3.(R,S)	5.25
	2.(S)	47.48

The mixture W-1000 is a eutectic mixture prepared from two chiral rod-like compounds with a phenyl biphenyl core and a terminal perfluoroalkoxyalkoxy chain, differing, however, in the length of the oligomethylene spacer 7 and 5, respectively, and the different position of the fluorine atom in the rigid core. For this mixture, we observed the following phase sequence, as shown in Scheme 1:

$$\text{SmC}_A^* \xrightarrow{\ T_1\ } \text{SmC}^* \xrightarrow{\ T_2\ } \text{SmA}^* \xrightarrow{\ T_3\ } \text{Iso}$$

Scheme 1. The designation of phase sequence and temperatures.

### 3. Results and Discussion

3.1. Mesomorphic Properties of Mixtures

Phase transitions and phase sequences were observed using the polarizing microscope (OLYMPUS BX51, Japan), which was equipped with a heating stage (Linkam THMS-600) and temperature controller (Linkam TMS-93). Observations were performed over the heating and cooling cycle at 2 °C/min. The phase transition temperatures were confirmed using a calorimeter NETZSCH, model STA 449F5 JUPITER (Germany). The measurements were carried out in the heating and cooling cycles in temperatures ranging from 30 °C to 120 °C, with a temperature change of 2 °C per minute in an argon atmosphere. The weight of each sample was 10 mg. Phase transition temperatures from microscopic and DSC measurements are compared in Table 4. One type of phase transition sequence can be observed regardless of the amount of racemate added; examples of the observed microphotograph textures of the smectic phases for one of the mixtures are shown in Figure 3. All phases were easily recognized based on microscopic textures without resorting to other identification methods. All prepared mixtures had similar transition temperatures, as shown in Figure 4. The enthalpies from the DSC measurements are compared in Table 5.

Table 4. Phase transition temperatures of all mixtures from the optical polarizing microscope and the differential scanning calorimeter.

Mixtures	SmC$_A$*	T$_1$	SmC*	T$_2$	SmA*	T$_3$	Iso
W-462	●	98.7–98.8	●	101.2–101.6	●	104.9–106.7	●
		96.1–96.9		100.7–101.5		103.8–105.7	
		96.6		99.3		102.8	
		93.2		98.0		101.0	
W-463	●	97.1–98.1	●	99.1–100.0	●	101.7–103.7	●
		93.2–95.6		98.5–99.0		100.6–102.8	
		97.4		99.4		102.8	
		94.9		98.2		100.8	
W-464	●	97.3–97.6	●	99.0–99.6	●	101.5–103.5	●
		95.4–96.1		98.5–99.1		100.6–102.5	
		97.9		99.7		102.6	
		95.6		98.3		100.7	
W-1000	●	100.5	●	103.6	●	106.1	●
		101.7		103.4		105.7	
		99.8		101.3		103.3	
		98.2		101.2		102.4	

First row: POM measurements in the heating cycle [°C]. Second row: POM measurements in the cooling cycle [°C]. Third row: DSC measurements in the heating cycle [°C]. Fourth row: DSC measurements in the cooling cycle [°C].

(**a**)

(**b**)

(**c**)
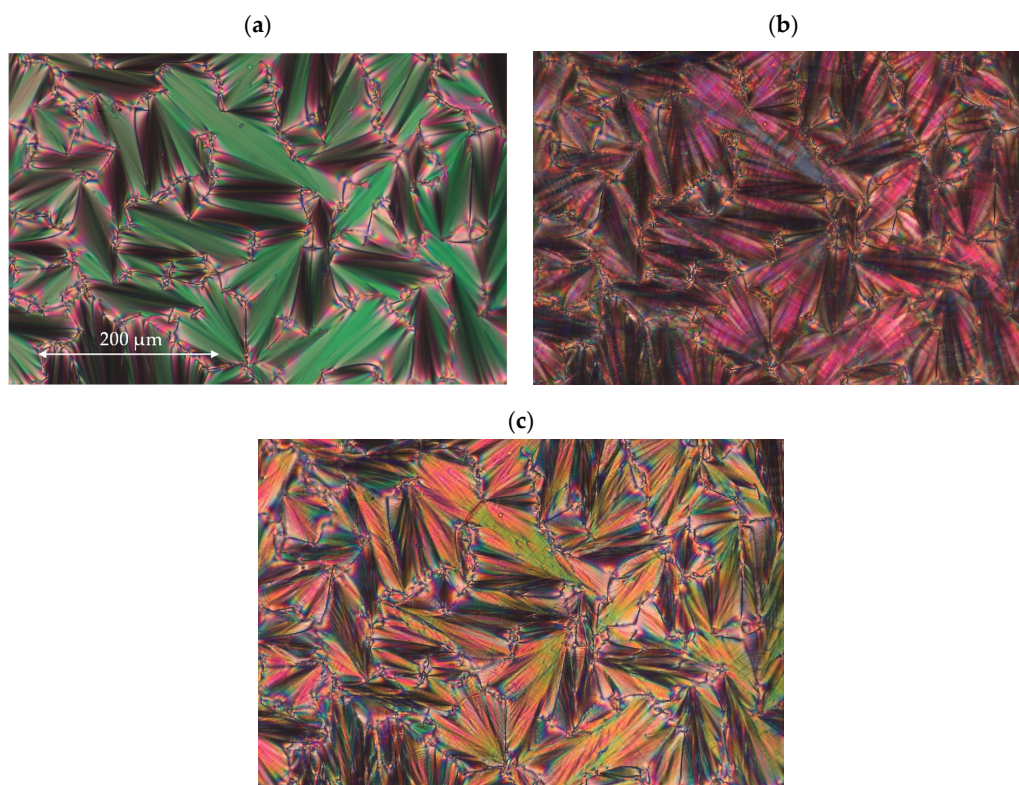
Figure 3. Photos of microscopic textures obtained for different mesophases for the mixture W-462: (**a**) SmA* phase at T = 103.8 °C; (**b**) SmC* phase at T = 100.7 °C; and (**c**) SmC$_A$* phase at T = 96.1 °C on the cooling cycle. The width of all microphotographs corresponds to ~600 μm.
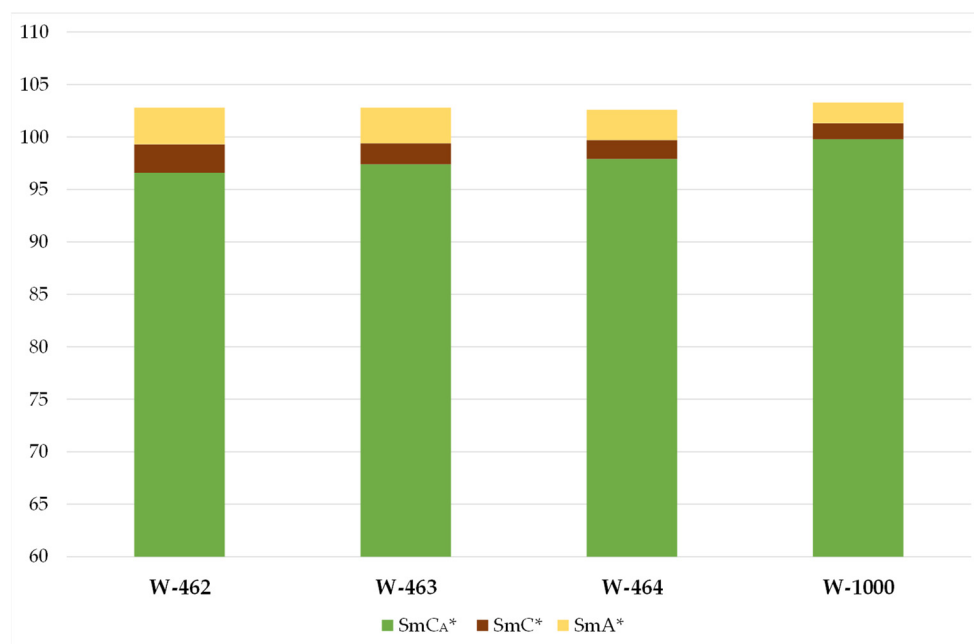
Figure 4. The temperatures of phase transition of all liquid crystalline mixtures from DSC measurements observed during the heating cycle (from 60 °C to 110 °C).

Table 5. Values of phase transition enthalpies for the mixture W-1000 and new mixtures (in the heating cycle).

	Mixture W-1000 [J/g]	Mixture W-462 [J/g]	Mixture W-463 [J/g]	Mixture W-464 [J/g]
SmC_A*-SmC*	0.11	0.03	0.06	0.07
SmC*-SmA*	1.19	1.05	1.03	0.89
SmA*-Iso	4.80	4.63	4.55	4.41

All the prepared mixtures have a wide temperature range in the antiferroelectric phase, while the ferroelectric phase and the smectic A* phase exist in a narrow temperature range. Comparing the obtained results with the phase transition temperatures of the base mixture W-1000, it can be seen that the mixture W-1000 is characterized by a narrower range of the SmC* and SmA* phases than the prepared mixtures. Comparing all three prepared mixtures with each other, the chiral smectic phase with ferroelectric properties and the SmA* phase occurs in the widest temperature range for the mixture W-462, where the addition of the racemate reaches the highest percentage value (50%). The narrowest range of these liquid crystalline phases appears for the mixture W-464, where the percentage of the racemate is 10%.

The clearing points for all mixtures are similar, with the prepared mixtures having slightly lower clearing points than the mixture W-1000 (by approximately 1–2 °C). It was impossible to determine the mixtures' melting or crystallization temperatures because the measurements were performed from 30 °C (the air-cooled measurement system).

The mixture W-1000 has higher phase transition enthalpies than the three new mixtures. In the case of the new mixtures, we observe a certain irregularity because the mixture W-464 (with the lowest percentage of the racemate) has the lowest enthalpy values, and the mixture W-462 (with the highest percentage of the racemate) has the highest values for the transitions: SmC*-SmA*, and SmA*-Iso. The transition SmC_A*–SmC* is characterized by very low enthalpy values both for the base mixture and for the new mixtures, which is why it is difficult to compare them as the differences are negligible.

3.2. Helical Pitch of Mixtures

The helical pitch was determined using the standard optical technique [38], which resorts to selective reflection. A free drop of the liquid crystalline mixture was placed on a glass plate coated with a CTAB (cetyltrimethylammonium bromide) layer, ensuring homeotropic order. A LIGA spectrophotometer was used for the research, enabling measurement in the UV–VIS range in transmitted light. The transmittance was measured as a function of wavelength. The pitch p was calculated for the antiferroelectric phase from the dependence:

$$\lambda_{max} = n \cdot p \tag{1}$$

The pitch p was calculated for he ferroelectric phase from the dependence:

$$\lambda_{max} = 2n \cdot p \tag{2}$$

where n is the average refractive index, the value n = 1.5 was taken to calculate [39]. The results were obtained during the cooling cycle.

The values of the dependence of light transmittance on the wavelength of selective reflection did not allow for the determination of the helical pitch in the tested spectral range (380–790 nm) for the mixture W-462, as shown in Figure 5.
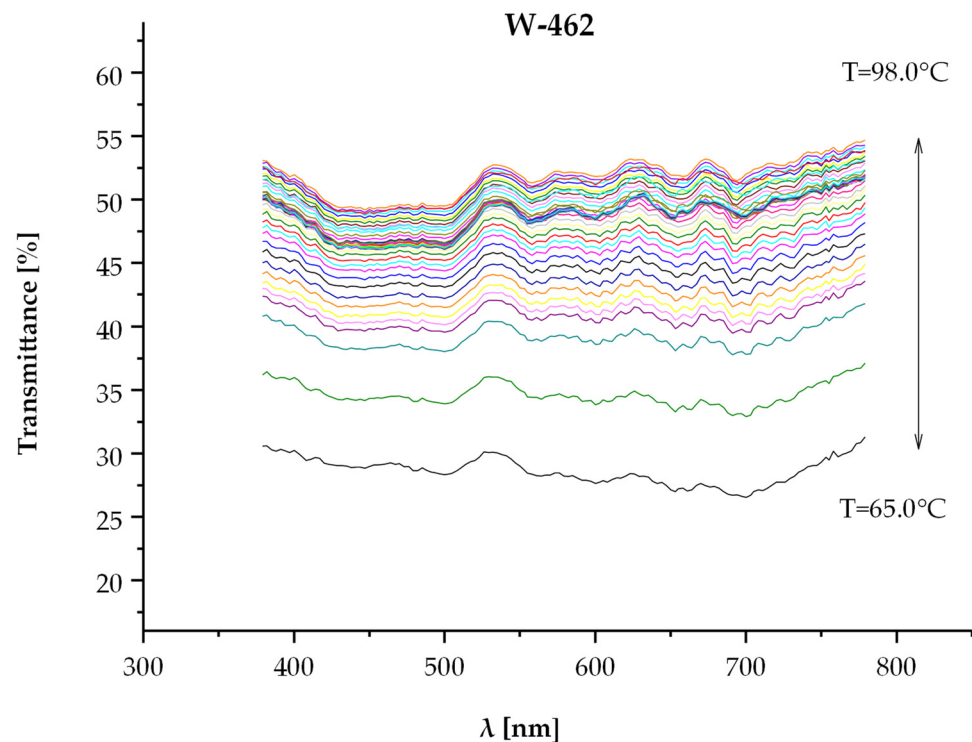

Figure 5. The dependence of transmittance on wavelength for the mixture W-462.

Based on the analysis of the UV–VIS spectrum and selective light reflection for the mixture W-463, the value of the selective reflection wavelength does not change significantly at the tested temperatures. It is in the range of 715.41 nm and 730.17 nm in the temperature range from 99.8 °C to 86.5 °C in the cooling cycle, as shown in Figure 6.
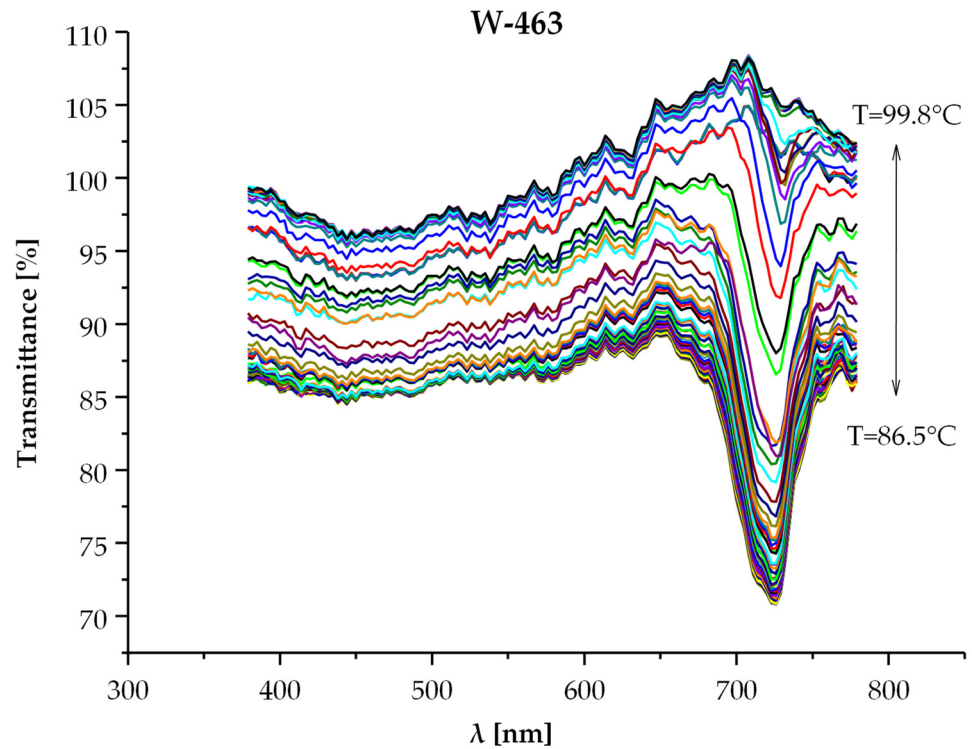
Figure 6. The dependence of transmittance on wavelength for the mixture W-463.

In the mixture W-464, selective reflection appears in the temperature range from 99.0 °C to 96.5 °C in the cooling cycle, and is approximately 661 nm. No selective reflection was observed above or below this temperature range, as shown in Figure 7.
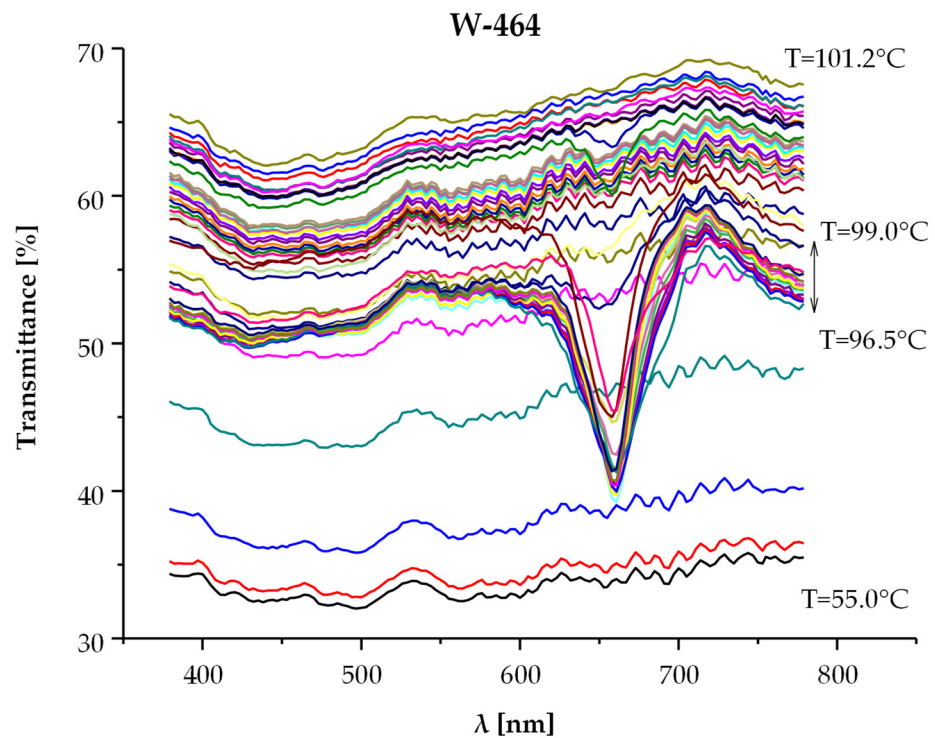

Figure 7. The dependence of transmittance on wavelength for the mixture W-464.

On this basis, the helical pitch in the ferroelectric phase for the mixture W-463 can be calculated at p = 318–324 nm (approx. 320 nm), and for the mixture W-464, the helical

pitch is 294 nm. Figure 8 shows the dependence of the helical pitch on temperature for the mixtures W-1000, W-463, and W-464. The helical pitch could not be determined for new mixtures in the antiferroelectric phase. The pitch values are outside the measurement range of the spectrophotometer used, so they cannot be compared with the pitch for the base mixture. As can be seen, the mixture W-1000 shows the inversion of the helical pitch in the SmC$_A$* phase. Above 20 °C, the helical pitch exceeds the value of 1000 nm. In the SmC* phase, the pitch values are outside the measurement range of the spectrophotometer used.
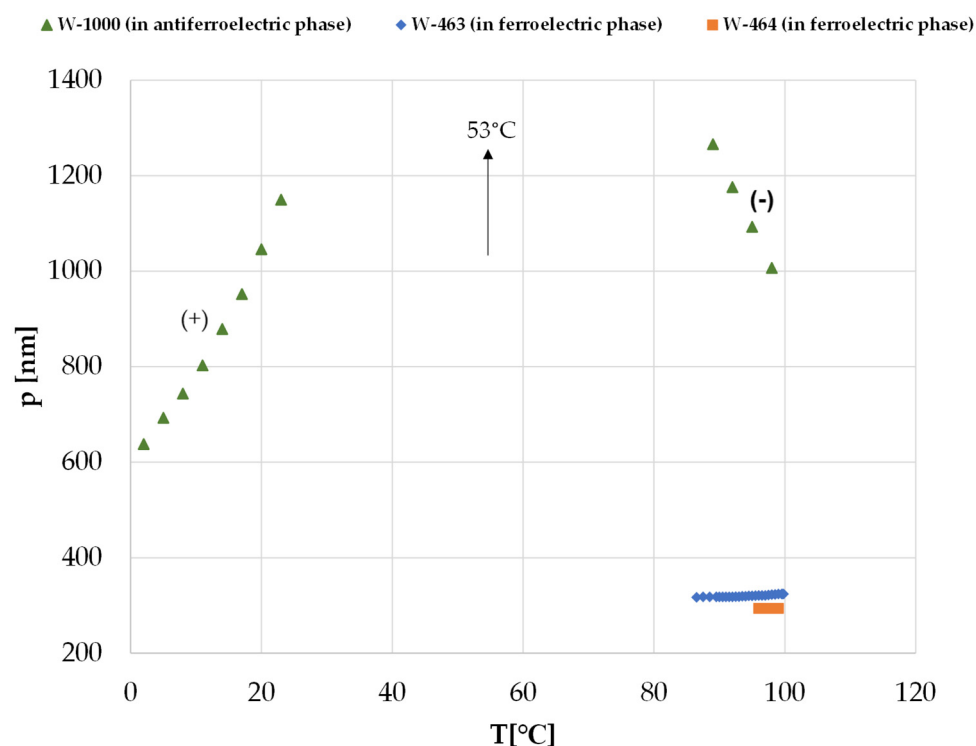

Figure 8. The helical pitch versus temperature for the mixtures W-1000, W-463, and W-464. ("(+)"- right-handed helix, "(-)"- left-handed helix). The arrow indicates the temperature at which the helix is unwound.

As expected, adding optically inactive mesogen to the base mixture causes an increase in the helical pitch in the SmC$_A$* phase, which has been observed previously [33–35,40–42].

4. Summary and Conclusions

Both chiral and achiral (racemic) materials have great application significance, which has been proven many times [43–50]. The influence of adding the racemate to the mixture on the physicochemical properties and helical pitch was confirmed in this study, which aimed to prepare three mixtures containing (S) enantiomers and racemate, examine their mesomorphic and thermodynamic properties and helical pitch, and compare them with the base mixture. All newly prepared mixtures have a wide temperature range in the antiferroelectric (SmC$_A$*) phase, while the ferroelectric (SmC*) phase and the smectic A* phase exist in a narrow temperature range. The temperature ranges of phase transitions and the clearing points for the prepared mixtures are comparable to those occurring for the mixture W-1000. The temperature ranges of the SmC* phase are wider by 1.2 °C, 0.5 °C, and by 0.3 °C for the mixtures W-462, W-463, and W-464, respectively, compared to the mixture W-1000. The temperature ranges of the SmA* phase are wider by 1.5 °C, 1.4 °C, and 0.9 °C for the mixtures W-462, W-463, and W-464, respectively, compared to the W-1000 mixture. The enthalpy values of phase transitions of the prepared mixtures are lower than those for the mixture W-1000. The helical pitch in the SmC* phase for the mixture W-463 is from 318 nm to 324 nm (approx. 320 nm); for the mixture W-464, the pitch is 294 nm. The

helical pitch is short in the ferroelectric phase and does not change upon heating. In the SmC_A^* phase, the pitch exceeds the measurement range of the spectrophotometer used.

The presented results are promising from an application point of view. Since the mixture W-1000 is orthoconic [51–56], electro-optical measurements (spontaneous polarization and tilt angle of molecules) will be performed for the newly developed mixtures in further stages of the research. At room temperature, the tilt angle for the mixture W-1000 is $\approx$43–45°. The spontaneous polarization of this mixture decreases with increases in temperature, reaching a maximum of almost 300 nC/cm^2 [29].

It can be concluded that adding the racemate to the chiral mixture positively affects the new mixtures' mesomorphic properties and helical pitch. For these mixtures, we observed a wide range of the SmC_A^* phase (ideally, only this phase would be present, and there would be no other smectic phases) [12], and low clearing points. The helical pitch is, in turn, one of the basic parameters determining the possibilities of using OAFLC materials. The pitch of most OAFLCs is below one μm, which makes OAFLCs difficult to stabilize on the surface. This also causes an asymmetry in the electro-optical response. Therefore, we look for materials with a longer helical pitch by adding different amounts of the racemate to the chiral base mixture.

The racemates can be successfully used as components or admixtures for the antiferroelectric chiral mixtures, which has also been demonstrated in other works [40–42].

Author Contributions: Conceptualization, M.U.; methodology, M.U.; software, M.U.; validation, M.U.; formal analysis, M.U.; resources, M.U. and D.D.; investigation, M.U. and D.D.; data curation, M.U. and D.D.; writing—original draft preparation, M.U. and D.D.; writing—review and editing, M.U. All authors have read and agreed to the published version of the manuscript.

References

1. Lagerwall, J.P.F.; Scalia, G. A new era for liquid crystal research: Applications of liquid crystals in soft matter nano-, bio- and microtechnology. *Curr. Appl. Phys.* **2012**, *12*, 1387–1412. [CrossRef]
2. D'have, K.; Rudquist, P.; Lagerwall, S.T.; Pauwels, H.; Drzewiński, W.; Dąbrowski, R. Solution of the dark state problem in antiferroelectric liquid crystal displays. *Appl. Phys. Lett.* **2000**, *76*, 3528–3530. [CrossRef]
3. Castillo, P.L.; Otón, J.M.; Dąbrowski, R.; Lara, A.; Quintana, X.; Bennis, N. Electrooptics of antiferroelectric orthoconic reflective displays. *Proc. SPIE* **2004**, *5565*, 284–289. [CrossRef]
4. Lagerwall, J.P.F.; Giesselmann, F. Current topics in smectic liquid crystal research. *ChemPhysChem* **2006**, *7*, 20–45. [CrossRef]
5. Clark, N.A.; Lagerwall, S.T. Submicrosecond bistable electro-optic switching in liquid crystals. *Appl. Phys. Lett.* **1980**, *36*, 899–901. [CrossRef]
6. Otón, J.M.; Quintana, X.; Castillo, P.L.; Lara, A.; Urruchi, V.; Bennis, N. Antiferroelectric liquid crystal displays. *Opto-Electr. Rev.* **2004**, *12*, 263–269.
7. Dąbrowski, R.; Kula, P.; Raszewski, Z.; Piecek, W.; Otón, J.M.; Spadło, A. New orthoconic antiferroelectrics useful for applications. *Ferroelectr.* **2010**, *395*, 116–132. [CrossRef]
8. Fitas, J.; Marzec, M.; Tykarska, M.; Wróbel, S.; Dąbrowski, R. Ferroelectric liquid crystal for use in a new generation of LCDs. *Acta Phys. Pol. A* **2013**, *124*, 954–958. [CrossRef]
9. Meyer, R.B. Ferroelectric liquid crystals; a review. *Mol. Cryst. Liq. Cryst.* **1977**, *40*, 33–48. [CrossRef]
10. Fukuda, A.; Takanishi, Y.; Isozaki, T.; Ishikawa, K.; Takezoe, H. Antiferroelectric chiral smectic liquid crystals. *J. Mat. Chem.* **1994**, *4*, 997–1016. [CrossRef]
11. Chandani, A.D.L.; Górecka, E.; Ouchi, Y.; Takezoe, H.; Fukuda, A. Antiferroelectric chiral smectic phases responsible for the tristable switching in MHPOBC. *Jap. J. Appl. Phys.* **1989**, *28*, L1265–L1268. [CrossRef]

12. Żurowska, M.; Morawiak, P.; Piecek, W.; Czerwiński, M.; Spadło, A.; Bennis, N. A new mesogenic mixture with antiferroelectric phase only at a broad temperature range. *Liq. Cryst.* **2016**, *43*, 1365–1374. [CrossRef]

13. Wang, J.; Bergquist, L.; Hwang, J.-I.; Kim, K.-J.; Lee, J.-H.; Hegmann, T.; Jákli, A. Wide temperature-range, multi-component, optically isotropic antiferroelectric bent-core liquid crystal mixtures for display applications. *Liq. Cryst.* **2018**, *45*, 333–340. [CrossRef]

14. Agrahari, A.; Nautiyal, V.K.; Vimal, T.; Pandey, S.; Kumar, S.; Manohar, R. Modification in different physical parameters of orthoconic antiferroelectric liquid crystal mixture via the dispersion of hexanethiol capped silver nanoparticles. *J. Mol. Liq.* **2021**, *332*, 115840. [CrossRef]

15. Mykytyuk, Z.M.; Barylo, H.I.; Kremer, I.P.; Kachurak, Y.M. Sensitive liquid crystal composites for optical sensors. *Mol. Cryst. Liq. Cryst.* **2024**, *768*, 1–8. [CrossRef]

16. Bubnov, A.; Tykarska, M.; Hamplová, V.; Kurp, K. Tuning the phase diagrams: The miscibility studies of multilactate liquid crystalline compounds. *Phase Trans.* **2016**, *89*, 885–893. [CrossRef]

17. Fitas, J.; Marzec, M.; Szymkowiak, M.; Jaworska-Gołąb, T.; Deptuch, A.; Tykarska, M.; Kurp, K.; Żurowska, M.; Bubnov, A. Mesomorphic, electro-optic and structural properties of binary liquid crystalline mixtures with ferroelectric and antiferroelectric liquid crystalline behaviour. *Phase Trans.* **2018**, *91*, 1017–1026. [CrossRef]

18. Czerwiński, M.; Tykarska, M. Helix parameters in bi- and multicomponent mixtures composed of orthoconic antiferroelectric liquid crystals with three ring molecular core. *Liq. Cryst.* **2014**, *41*, 850–860. [CrossRef]

19. Knapkiewicz, M.; Robakowska, M.; Rachocki, A. Thermal stabilization of the smectic-C$_\alpha$* phase by doping with photo-active reactive mesogen. *J. Mol. Liq.* **2022**, *361*, 119552. [CrossRef]

20. Tomczyk, W.; Marzec, M.; Juszyńska-Gałązka, E.; Węgłowska, D. Mesomorphic and physicochemical properties of liquid crystal mixture composed of chiral molecules with perfluorinated terminal chains. *J. Mol. Struct.* **2017**, *1130*, 503–510. [CrossRef]

21. Debnath, A.; Mandal, P.K. Effect of fluorination on the phase sequence, dielectric and electro-optical properties of ferroelectric and antiferroelectric mixtures. *Liq. Cryst.* **2017**, *44*, 2192–2202. [CrossRef]

22. Czerwiński, M.; de Blas, M.G.; Bennis, N.; Herman, J.; Dmochowska, E.; Otón, J.M. Polymer stabilized highly tilted antiferroelectric liquid crystals—The influence of monomer structure and phase sequence of base mixtures. *J. Mol. Liq.* **2020**, *327*, 114869. [CrossRef]

23. Shi, F.; Han, F.; Zhang, W.; Yang, Y.; Li, H. Color-tunable circularly polarized luminescence from liquid crystalline polymer networks. *Dyes Pigm.* **2024**, *222*, 111910. [CrossRef]

24. Ma, J.; Xuan, L. Towards nanoscale molecular switch-based liquid crystal displays. *Displays* **2013**, *34*, 293–300. [CrossRef]

25. Lalik, S.; Deptuch, A.; Fryń, P.; Jaworska-Gołąb, T.; Węgłowska, D.; Marzec, M. Physical properties of new binary ferroelectric mixture. *J. Mol. Liq.* **2019**, *274*, 540–549. [CrossRef]

26. Milewska, K.; Drzewiński, W.; Czerwiński, M.; Dąbrowski, R.; Piecek, W. Highly tilted liquid crystalline materials possessing a direct phase transition from antiferroelectric to isotropic phase. *Mat. Chem. Phys.* **2016**, *171*, 33–38. [CrossRef]

27. Hird, M. Ferroelectricity in liquid crystals—Materials, properties and applications. *Liq. Cryst.* **2011**, *38*, 1467–1493. [CrossRef]

28. Dardas, D. Tuning the electro-optic and viscoelastic properties of ferroelectric liquid crystalline materials. *Rheo. Acta* **2019**, *58*, 193–201. [CrossRef]

29. Piecek, W.; Perkowski, P.; Raszewski, Z.; Morawiak, P.; Żurowska, M.; Dąbrowski, R.; Czupryński, K. Long Pitch Orthoconic Antiferroelectric Binary Mixture for Display Applications. *Mol. Cryst. Liq. Cryst.* **2010**, *525*, 160–172. [CrossRef]

30. Perkowski, P.; Ogrodnik, K.; Piecek, W.; Raszewski, Z.; Żurowska, M.; Dąbrowski, R. High frequency mode in new antiferroelectric mixture. *Mol. Cryst. Liq. Cryst.* **2010**, *525*, 50–56. [CrossRef]

31. Perkowski, P.; Piecek, W.; Raszewski, Z.; Ogrodnik, K.; Żurowska, M.; Dąbrowski, R.; Kędzierski, J. Precise dielectric spectroscopy of a long pitch orthoconic antiferroelectric working mixture. *Mol. Cryst. Liq. Cryst.* **2011**, *541*, 191–200. [CrossRef]

32. Chełstowska, A.; Czerwiński, M.; Tykarska, M.; Bennis, N. The influence of antiferroelectric compounds on helical pitch of orthoconic W-1000 mixture. *Liq. Cryst.* **2014**, *41*, 812–820. [CrossRef]

33. Ogrodnik, K.; Perkowski, P.; Raszewski, Z.; Piecek, W.; Żurowska, M.; Dąbrowski, R.; Jaroszewicz, L. Dielectric Measurements of Orthoconic Antiferroelectric Liquid Crystal Mixtures. *Mol. Cryst. Liq. Cryst.* **2011**, *547*, 54–64. [CrossRef]

34. Morawiak, P.; Żurowska, M.; Piecek, W. A Long Pitch Orthoconic Antiferroelectric Mixture Modified by Isomeric and Racemic Homostructural Dopants. *Liq. Cryst.* **2018**, *45*, 1451–1459. [CrossRef]

35. Piecek, W.; Dąbrowski, R.; Morawiak, P.; Żurowska, M.; Jaroszewicz, L. The orthoconic antiferroelectric smectic liquid crystals and their engineering by doping with homo- and heterostructural compounds. *Phase Trans.* **2012**, *85*, 910–929. [CrossRef]

36. Żurowska, M.; Dąbrowski, R.; Dziaduszek, J.; Skrzypek, K.; Filipowicz, M.; Rejmer, W.; Czupryński, K.; Bennis, N.; Otón, J.M. Influence of alkoxy chain length and fluorosubstitution on mesogenic and spectral properties of high tilted antiferroelectric esters. *J. Mat. Chem.* **2011**, *21*, 2144–2153. [CrossRef]

37. Urbańska, M.; Dziaduszek, J.; Strzeżysz, O.; Szala, M. Synclinic and anticlinic properties of (R,S) 4′-(1-methylheptyloxycarbonyl)biphenyl-4-yl 4-[7-(2,2,3,3,4,4,4-heptafluorobutoxy)heptyl-1-oxy]benzoates. *Phase Trans.* **2019**, *92*, 657–666. [CrossRef]

38. Dardas, D.; Kuczyński, W. Non-linear electrooptical effects in chiral liquid crystals. *Opto-Electr. Rev.* **2004**, *12*, 277–280.

39. Raszewski, Z.; Kędzierski, J.; Perkowski, P.; Piecek, W.; Rutkowska, J.; Kłosowicz, S.; Zieliński, J. Refractive indices of the MHPB(H)PBC and MHPB(F)PBC antiferroelectric liquid crystals. *Ferroelectrics* **2002**, *276*, 289–300. [CrossRef]

40. Urbańska, M.; Szala, M. Synthesis, Mesomorphic Properties and Application of (R,S)-1-Methylpentyl 4′-Hydroxybiphenyl-4-carboxylate Derivatives. *Crystals* **2022**, *12*, 1710. [CrossRef]

41. Verma, R.; Dąbrowski, R.; Żurowska, M.; Dhar, R. Enhancement of the properties and mesophases stability after the electron beam irradiation on a racemic anti-ferroelectric liquid crystalline mixture. *Liq. Cryst.* **2016**, *43*, 606–614. [CrossRef]
42. Żurowska, M.; Dąbrowski, R.; Dziaduszek, J.; Rejmer, W.; Czupryński, K.; Raszewski, Z.; Piecek, W. Comparison of Racemic and Enantiomeric 4′-(1-Methylheptyloxycarbonyl)Biphenyl-4-yl 4-[3-(2,2,3,3,4,4,4-Heptafluorobutoxy)Prop-1-Oxy]Benzoates. *Mol. Cryst. Liq. Cryst.* **2010**, *525*, 219–225. [CrossRef]
43. Guo, J.; Xue, X.; Li, F.; Zhao, M.; Xing, Y.; Song, Y.; Long, C.; Zhao, T.; Liu, Y.; Tang, Z. Modulation of the assembly fashion among metal–organic frameworks for enantioretentive epoxide activation. *Nanoscale Horiz.* **2024**, *9*, 118–122. [CrossRef] [PubMed]
44. Gao, J.; Zhen, Y.; Yu, W.; Wang, Y.; Jin, T.; Pan, X.; Loh, K.P.; Chen, W. Intrinsic polarization coupling in 2D α-In$_2$Se$_3$ toward artificial synapse with multimode operations. *SmartMat* **2021**, *2*, 88–98. [CrossRef]
45. Guo, J.; Duan, Y.; Jia, Y.; Zhao, Z.; Gao, X.; Liu, P.; Li, F.; Chen, H.; Ye, Y.; Liu, Y.; et al. Biomimetic chiral hydrogen-bonded organic-inorganic frameworks. *Nat. Comm.* **2024**, *15*, 139. [CrossRef] [PubMed]
46. Burmistrov, V.; Novikov, I.; Aleksandriiskii, V.; Batrakova, A.; Belykh, D.; Startseva, O.; Koifman, O.I. Chiral induction of helical mesophase by amphiphilic chlorin e6 derivatives and their metal complexes: Effect of chiral and achiral aliphatic chains. *J. Mol. Liq.* **2024**, *396*, 123957. [CrossRef]
47. Rapeenun, P.; Gerard, C.J.J.; Pinètre, C.; Cartigny, Y.; Tinnemans, P.; de Gelder, R.; Flood, A.E.; ter Horst, J.H. Searching for Conglomerate Cocrystals of the Racemic Compound Praziquantel. *Cryst. Growth Des.* **2024**, *24*, 480–490. [CrossRef]
48. Kovač, J.; Vargas, M.; Keiser, J. In vitro and in vivo activity of R- and S- praziquantel enantiomers and the main human metabolite trans-4-hydroxy-praziquantel against Schistosoma haematobium. *Parasites Vect.* **2017**, *10*, 365. [CrossRef]
49. Pieraccini, S.; Ferrarini, A.; Spada, G.P. Chiral Doping of Nematic Phases and Its Application to the Determination of Absolute Configuration. *Chirality Pharmacol. Biol. Chem. Conseq. Mol. Asymmetry* **2008**, *20*, 749–759. [CrossRef]
50. Cook, M.J.; Wilson, M.R. Calculation of helical twisting power for liquid crystal chiral dopants. *J. Chem. Phys.* **2000**, *112*, 1560–1564. [CrossRef]
51. D'havé, K.; Dahlgren, A.; Rudquist, P.; Lagerwall, J.P.F.; Andersson, G.; Matuszczyk, M.; Lagerwall, S.T.; Dąbrowski, R.; Drzewiński, W. Antiferroelectric Liquid Crystals with 45° Tilt—A New Class of Promising Electro-Optic Materials. *Ferroelectrics* **2000**, *244*, 115–128. [CrossRef]
52. Lagerwall, S.T.; Dahlgren, A.; Jagemalm, P.; Rudquist, P.; D'Have, K.; Pauwels, H.; Dąbrowski, R.; Drzewiński, W. Unique electro-optical properties of liquid crystals designed for molecular optics. *Adv. Funct. Mat.* **2001**, *11*, 87–94. [CrossRef]
53. Rudquist, P.; Meier, J.G.; Lagerwall, J.P.F.; D'have, K.; Lagerwall, S.T. Tilt plane orientation in antiferroelectric liquid crystal cells and the origin of the pretransitional effect. *Phys. Rev. E* **2002**, *66*, 1–10. [CrossRef] [PubMed]
54. Rudquist, P. Orthoconic antiferroelectric liquid crystals. *Liq. Cryst.* **2013**, *40*, 1678–1697. [CrossRef]
55. Dąbrowski, R.; Gąsowska, J.; Otón, J.; Piecek, W.; Przedmojski, J.; Tykarska, M. High tilted antiferroelectric liquid crystalline materials. *Displays* **2004**, *25*, 9–19. [CrossRef]
56. Drzewiński, W.; Dąbrowski, R.; Czupryński, K. Orthoconic antiferroelectrics. Synthesis and mesomorphic properties of optically active (S)-(+)-4-(1-methylheptyloxycarbonyl)phenyl 4′-(fluoroalkanoyloxyalkoxy)biphenyl-4-carboxylates and 4′-(alkanoyloxyalkoxy)biphenyl-4-carboxylates. *Pol. J. Chem.* **2002**, *76*, 273–284. [CrossRef]